Quantum dimer calculations on the spin-$\frac{1}{2}$ *kagomé* Heisenberg antiferromagnet

Chen Zeng*
Department of Mathematics, University of Manchester Institute of Science and Technology (UMIST)
P.O. Box 88, Manchester M60 1QD, United Kingdom
and Department of Physics, Cornell University, Ithaca, New York 14853-2501

Veit Elser
Department of Physics, Cornell University, Ithaca, New York 14853-2501
(Received 26 September 1994; revised manuscript received 21 November 1994)

In analogy to the quantum dimer model on the square lattice introduced by Rokhsar and Kivelson, we identify the low-energy Hilbert space of the spin-$\frac{1}{2}$ *kagomé* Heisenberg antiferromagnet with the set of dimerized states (nearest-neighbor singlets) and derive an effective Hamiltonian which describes resonance and includes fluctuations into next-nearest-neighbor singlets. Complete diagonalization of this effective Hamiltonian for systems as large as 36 spins makes possible the study of the low-energy thermodynamics of this quantum antiferromagnet and strongly supports the double peak feature in the heat capacity.

I. INTRODUCTION

The quantum dimer model (QDM) was introduced by Rokhsar and Kivelson[1] for the $S = \frac{1}{2}$ square lattice Heisenberg antiferromagnet (HAF) as an alternative description of a possible non-Néel state. There are two essential ingredients of simplification in this approach: First of all, the low-energy Hilbert space is identified with a set of dimerized (nearest-neighbor singlet) states. Rokhsar and Kivelson have argued that it is reasonable to truncate the full Hilbert space in this fashion, provided that spin-spin correlation functions are short ranged and a gap exists in the spin excitations which separates the low-lying excitations in the spin singlet sector from higher spin excitations. Second, an effective Hamiltonian within this restricted Hilbert space is made local by taking into account the resonance of the dimerized states to the lowest order, i.e., resonance over the shortest even-sided loops on the lattice. This simplification is somewhat drastic in the sense that the nonorthogonality of the dimerized states will induce resonances over arbitrarily large loops, albeit with exponentially decaying amplitudes.

As suggested by cluster studies[2] and others,[3,4] the quantum $S = \frac{1}{2}$ *kagomé* Heisenberg antiferromagnet (HAF) presumably has exponentially decaying spin-spin correlation functions[2–4] and a gap of about one-fourth of the exchange coupling constant for spin triplet excitations.[2] These features therefore make the QDM particularly suitable for the *kagomé* HAF. Furthermore, compared with the square lattice HAF, the *kagomé* structure, with its shortest even-sided loop being a hexagon, provides a smaller expansion parameter which may help to reduce the effect of the nonlocality of the effective Hamiltonian.

A recent high-order high-temperature expansion study on the $S = \frac{1}{2}$ *kagomé* HAF by Elstner and Young[6] shows unambiguously that the heat capacity has further structure at lower temperature in addition to a high-temperature peak. This puts the double-peak feature of the heat capacity first speculated by Elser[5] on firm ground. The detailed picture of the low-temperature heat capacity together with the nature of the low-temperature phase is, however, not easily accessible from the high-temperature expansion study. By identifying the low-energy Hilbert space of the spin-$\frac{1}{2}$ *kagomé* Heisenberg antiferromagnet with the set of dimerized states (nearest-neighbor singlets), we can derive an effective Hamiltonian for the low-energy singlet sector that can be diagonalized for systems as large as 36 spins. The studies of the low-energy thermodynamics from the present approach therefore complement the high-temperature expansion study.

Remarkably enough, the highly degenerate mean field solutions of the fermionic SU(N) generalization for the *kagomé* HAF are composed of the same set of dimerized states.[7] Fluctuation corrections at order $1/N$ corresponding to a fluctuating "benzene cluster" are responsible for freezing the singlet pairs into a pattern having a maximum number of such clusters.[8] For the physically relevant SU(2) case, it is important to investigate the stability of this "spin-solid" phase against higher-order corrections. This also motivates the present QDM calculations for the *kagomé* HAF.

In view of several approximations involved, we organize this paper as follows: In Sec. II, some terminology is introduced to characterize the manifold of the dimerized states in terms of a loop gas representation and a pseudospin representation. We specify the reduced Hilbert space to be used throughout this paper. An effective Hamiltonian within this reduced Hilbert space is briefly outlined in Sec. III, since detailed derivations can be found in Ref. 9. In this section, we also suggest a scheme

to classify the order of both overlap and Hamiltonian matrix elements in terms of a small expansion parameter ϵ. In Sec. IV, this effective Hamiltonian is truncated to the lowest nontrivial resonance order $O(\epsilon)$ by setting all the matrix elements of higher order in both overlap and Hamiltonian matrices to zero. This truncated Hamiltonian is numerically diagonalized for a 36-spin cluster, and the results are presented in this section. Since the Hilbert space is reduced, and the Hamiltonian truncated, we discuss the possible refinement on the basis by including next-nearest-neighbor singlets and the effect of higher-order resonance in Secs. V and VI, respectively. Finally, we summerize the present QDM calculations for the $S = \frac{1}{2}$ *kagomé* HAF in Sec. VII.

II. DIMERIZED STATES

The full Hilbert space is truncated to a set of dimerized states $\{|D\rangle\}$ which can be expressed as a tensor product of nearest-neighbor spin singlet pairs $[ij]$ between sites i and j:

$$|D\rangle = \prod_{(ij)} [ij] \ . \tag{1}$$

Since $[ij]$ is antisymmetric upon interchanging sites i and j, a direction must be specified for each singlet pair. The simplest choice is to orient the singlet pairs clockwise around the triangles. An arrow is assigned for each singlet pair to indicate this phase convention.

To see why a dimerized state fails to be the ground state of the *kagomé* HAF, we can rewrite the Hamiltonian in a more transparent form by adding a constant to the conventional definition as follows:

$$\begin{aligned} H &= \sum_{(ij)} \left(\mathbf{S}_i \cdot \mathbf{S}_j + \frac{1}{4} \right) \\ &= \sum_{(ijk)} \frac{3}{4} P_{\frac{3}{2}} (\mathbf{S}_i + \mathbf{S}_j + \mathbf{S}_k) \equiv \sum_{(ijk)} H_{ijk} \ . \end{aligned} \tag{2}$$

Here we have used (ij) and (ijk) to denote a bond and a triangle, respectively, on the *kagomé* structure in the above equations. Since the projection operator $P_{\frac{3}{2}}$ onto the highest total spin state of three mutually coupled spins on a triangle is positive semidefinite, the lowest energy (zero) is achieved on a triangle which has a singlet pair, because the total spin in that triangle can no longer reach its possible maximum of $\frac{3}{2}$ in the presence of the singlet pair. Unfortunately, this local minimum configuration cannot be fulfilled simultaneously on all triangles on the *kagomé* lattice. Therefore, a triangle without a singlet pair has a positive energy and is called a defect triangle (or simply a defect). A dimerized state with a finite number of defects is no longer an eigenstate of the Hamiltonian. It was also shown for the *kagomé* lattice that the total number of defects in a fully dimerized state is actually independent of dimerization.[5] The distribution of defects or the defect-defect interaction has to be calculated to probe the ground state ordering. A preponderance of one particular defect cluster, the smallest three-defect cluster (see Fig. 1), for example, would be the result of an attractive defect-defect interaction. To detect such clusters, we can measure the number of hexagons having three attached defects which will be called "perfect hexagons."

One way to describe the dimerized states is the transition graph representation constructed by superimposing two dimerized states $|D_1\rangle$ and $|D_2\rangle$ on the same lattice as done in Fig. 1. A transition graph represents an assembly of closed, nonintersecting loops (also called resonance loops).

Within this loop gas representation, it is rather natural to specify the order of the resonance loops by the number of hexagons enclosed, because the overlap matrix element for the smallest resonance loop, i.e., the hexagon, can be treated as a small expansion parameter (see next section). To the lowest order, there are eight topologically distinct resonance loops as displayed in Fig. 2.

This loop gas representation also reveals the topological relationship among the dimerized states. In a finite system with periodic boundary conditions, the transition graph formed by two dimerizations is characterized by two winding numbers (n_x, n_y) around the two-torus. Moreover, two resonance loops winding around the torus along the same direction, giving $n_x = 2$, can be continuously deformed to a removable loop ($n_x = 0$) by a series of local transformations of the singlet pairs. Topologically, the set of dimerized states decomposes into four equivalent sectors denoted by $(n_x, n_y) = (0,0)$, $(0,1)$, $(1,0)$, and $(1,1)$, respectively. For a 36-spin cluster, for example, we decompose all 8192 dimerized states into four sectors, each of which has a dimension of 2048. In the thermodynamic limit, these sectors are disconnected because the corresponding overlap and Hamiltonian matrix elements become zero. As a further approximation for finite clusters, we confine ourselves to the further reduced Hilbert space which consists of all the states in the single sector $(n_x, n_y) = (0,0)$ with respect to the reference state $|D_1\rangle$ shown in Fig. 1. All the numerical results reported throughout this paper are obtained in

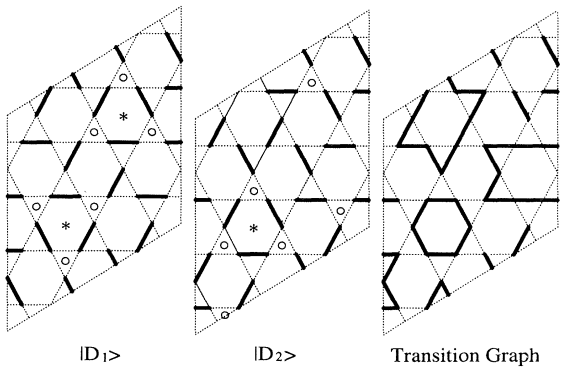

FIG. 1. Two different dimerized states $|D_1\rangle$ and $|D_2\rangle$ on a 36-spin cluster for the *kagomé* structure with periodic boundary conditions, along with their corresponding transition graph. Defects are indicated by ○; perfect hexagons are marked by ∗.

Resonance Loops	(1) 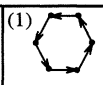	(2) 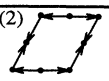	(3) 	(4) 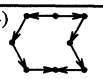
f_r	-1/4	1/8	1/8	1/8
g_r	3	2	2	2
$f_r g_r = h_r$	-3/4	1/4	1/4	1/4
Resonance Loops	(5) 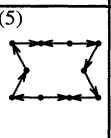	(6) 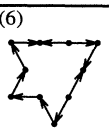	(7) 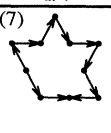	(8) 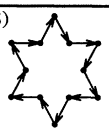
f_r	-1/16	-1/16	-1/16	1/32
g_r	1	1	1	0
$f_r g_r = h_r$	-1/16	-1/16	-1/16	0

FIG. 2. All eight topologically distinct resonance loops of lowest order. The arrows on the singlet pairs indicate the sign convention, and f_r, g_r, and h_r are used in Eq. (6) and Eq. (7).

this further reduced Hilbert space of dimension 2048.

For the *kagomé* structure, it was shown that the entropy of dimer coverings is equal to $(N/3)\ln 2$ where N denotes the total number of sites.[5] Since $N/3 = M$ is just the number of hexagons, this suggests that it is possible to represent the dimerized states by a set of Ising-like variables ($\sigma^z = \pm 1$) defined on hexagons as

$$\|D\rangle\rangle = \|\sigma_1^z, \ldots, \sigma_M^z, D_0\rangle\rangle \ , \tag{3}$$

where D_0 is a reference dimerized state, and the double ket symbol is introduced to differentiate this pseudospin representation from the conventional representation given in Eq. (1). The equivalence between this pseudospin representation and the loop gas representation can be seen easily by identifying the outcome of a single pseudospin flip at a given hexagon with the appearance of the corresponding lowest-order resonance loop at the same hexagon (see Fig. 2 for all eight topologically distinct lowest order resonance loops). Clearly, the equivalence holds only if the same reference dimerized state is used for both representations. Apart from clearly identifying the degrees of freedom in the reduced Hilbert space, the pseudospin representation in Eq. (3) uses a manifestly orthogonal basis.

III. MATRIX ELEMENTS AND EFFECTIVE HAMILTONIAN

The overlap matrix element between two dimerized states $|D_1\rangle$ and $|D_2\rangle$ can be evaluated by the following formula:

$$O_{D_1,D_2} = \langle D_1|D_2\rangle = 2\left(\frac{1}{\sqrt{2}}\right)^{l_1} \cdots 2\left(\frac{1}{\sqrt{2}}\right)^{l_n} \ , \tag{4}$$

where l_i denotes the length of the ith resonance loop between $|D_1\rangle$ and $|D_2\rangle$. This result comes about because for each loop, in order to have a nonzero contribution to the overlap matrix element, the spins in the loop for both dimerized states are completely fixed up to a global spin flip; therefore a factor of 2 comes from this freedom along with a normalization constant $\frac{1}{\sqrt{2}}$ from each singlet pair in the loop. A small parameter, namely, the overlap matrix element for the smallest resonance loop, $\epsilon = 2(\frac{1}{\sqrt{2}})^6 = \frac{1}{4}$ can be introduced. Therefore, a resonance loop enclosing m hexagons will be of order $O(\epsilon^m)$.

Similarly the Hamiltonian matrix elements can also be computed easily as

$$\begin{aligned} H_{D_1,D_2} &= \sum_{(ij)} \langle D_1| \left(\mathbf{S}_i \cdot \mathbf{S}_j + \frac{1}{4}\right) |D_2\rangle \\ &= \sum_{(ij)} \left\{\frac{3}{4} d_{ij} + \frac{1}{4}\right\} O_{D_1,D_2} \ , \end{aligned} \tag{5}$$

where d_{ij} equals 1 (-1) if sites i and j belong to the same loop and separated by an even (odd) number of singlet pairs, and 0 otherwise.

In terms of pseudospin representations, a straightforward calculation shows,[9] by directly examining the lowest-order resonance loops, that

$$\begin{aligned} O_{D_1,D_2} &= \delta_{D_1,D_2} + \langle\langle D_1\| \sum_r \sigma_r^x f_r \|D_2\rangle\rangle + O(\epsilon^2) \ , \\ H_{D_1,D_2} &= \Delta N_d \delta_{D_1,D_2} + \Delta \langle\langle D_1\| \sum_r \sigma_r^x f_r (N_d - g_r) \|D_2\rangle\rangle \\ &\quad + O(\epsilon^2) \ , \end{aligned} \tag{6}$$

where we have used N_d to indicate the number of defects, each of which has a defect energy $\Delta = 3/4$; also the sum is over all the hexagons (labeled by r), and f_r and g_r are listed in Fig. 2 for each resonance loop of order ϵ.

Furthermore, within the orthogonal basis $\{\|D\rangle\rangle\}$, which can be viewed as a linear transformation of the nonorthogonal basis $\{|D\rangle\}$, an effective Hamiltonian is given by

$$\begin{aligned} H_{\text{eff}} &= O^{-1/2} H O^{-1/2} \\ &= \Delta N_d - \Delta \sum_r \sigma_r^x h_r + O(\epsilon^2) \ . \end{aligned} \tag{7}$$

The physical interpretation of this effective Hamiltonian is evident: The first term corresponds to a potential energy measuring the total number of defects in the system, whereas the second term, a kinetic energy, describes the resonance effect with the tunneling amplitudes specified by $\{h_r \equiv f_r g_r\}$.

IV. GROUND STATE AND EXCITATIONS

For the set of nonorthogonal basis states $\{|D\rangle\}$, the energy spectrum $(\{E_n\})$ can be obtained by solving the generalized eigenvalue equation

$$H|\psi_n\rangle = E_n O|\psi_n\rangle \ , \tag{8}$$

where H and O are the energy and overlap matrices computed in Eqs. (4) and (5). Equivalently, we can also work

in the orthogonal basis $||D\rangle\rangle$ to diagonalize the effective Hamiltonian H_{eff} and obtain the same spectrum.

The introduction of this small expansion parameter ϵ in the previous section enables us to study the resonance effect order by order. In this section, only the lowest-order resonances are taken into account. To this end, we truncate both overlap and Hamiltonian matrices to the first resonance order $O(\epsilon)$ by keeping the terms explicitly given in Eq. (6) and Eq. (7) and setting all others to zero. The effect of higher-order resonances is to be studied in Sec. VI. Even to the lowest nontrivial order $O(\epsilon)$, the above eigenvalue problem is far from being analytically solvable because of all the competing energy scales $\{h_r\}$ associated with low-lying excitations in the spin singlet sector. We are therefore forced to resort to cluster studies. Here we numerically diagonalize Eq. (8) for the 36-spin cluster displayed in Fig. 1. The dimension of the Hamiltonian for this cluster is 2048. The energy spectrum is plotted in Fig. 3. A gap in the spectrum is clearly visible. To elucidate the nature of this gap, we also compute the average number of perfect hexagons, N_{6p}, in the corresponding eigenstates and plot the results in Fig. 4. First of all, the discontinuous jump in N_{6p} correlates precisely with the appearance of the gap which is very suggestive of a condensation of some sort. Second, it should be noted that the 36-spin cluster permits only zero, one, or two such perfect hexagons for each of its dimerized states. The expectation values of N_{6p} for the low-lying excitations below the gap are all very close to the maximum allowed value. From the above two observations in this cluster study to the lowest nontrivial order, we then speculate that a gap opens up in the excitation spectrum corresponding to a crystallization of spin singlet pairs into a phase with the maximum number of perfect hexagons. Since each perfect hexagon represents three tightly bound defects, then, to this order of approximation, the defect-defect interaction appears to be attractive.

Since the full spectrum is obtained, the heat capacity is readily computed and is shown in Fig. 5. It has

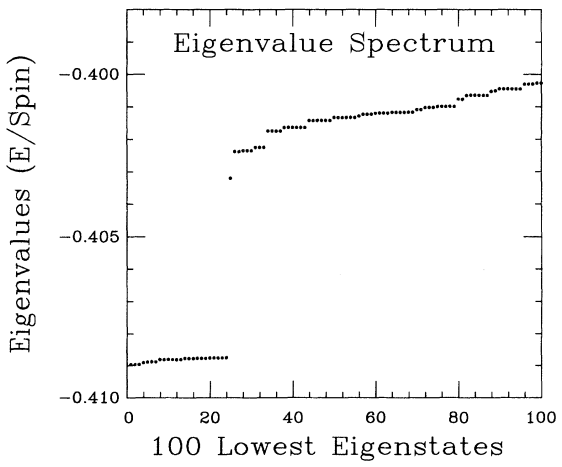

FIG. 3. The energy eigenvalues for the 100 lowest eigenstates, for the basis of nearest-neighbor singlet wave functions. The energy has been converted to the conventional definition.

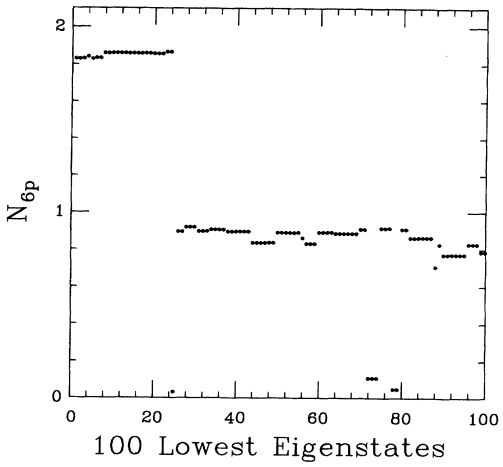

FIG. 4. The average number of perfect hexagons N_{6p} corresponding to the energy eigenstates of Fig. 3.

an exponentially decaying low-temperature behavior due to the gap. The peak position in the heat capacity at about 0.1 compares well with the location of the low-temperature peak of the heat capacity obtained for a 12-spin cluster;[5] the magnitude at the peak position is, however, only about 50% of that of the 12-spin cluster.

In terms of the conventional Hamiltonian [i.e., without the additive constant in Eq. (2)], the ground state energy per spin $E_0 = -0.4089$ is about 7% higher than the exact numerical result -0.4383 obtained by Leung and Elser[2] for the 36-spin cluster, indicating the inadequacy of the basis of the dimerized states in building a good trial wave function. This deficiency will be corrected in the next section where next-nearest-neighbor singlet pairs around defects are incorporated.

V. DEFECT FLUCTUATIONS AND REFINED BASIS

When the Hamiltonian acts on a state containing defects, the resulting state has an admixture of next-

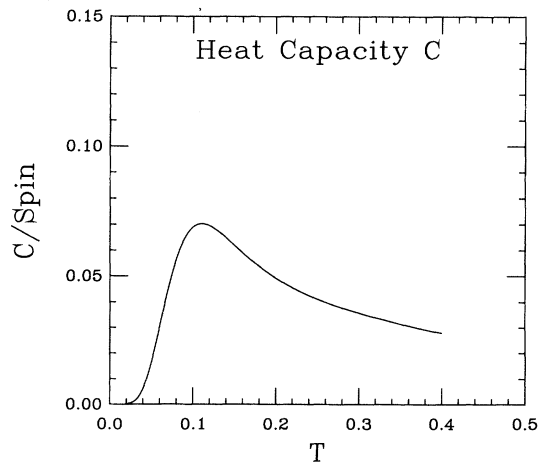

FIG. 5. Heat capacity obtained in basis of nearest-neighbor dimerized states.

nearest-neighbor singlet bonds in the vicinity of each defect. A good variational wave function must include such fluctuations in each of the dimerized states of the superposition. Incorporating these features, a class of refined basis states $\{|D_\alpha\rangle\}$, with one variational parameter α was proposed in Ref. 9 as

$$|D_\alpha\rangle = \prod_{\text{defects}-(ijk)} (1+\alpha H_{ijk})|D\rangle \ , \tag{9}$$

where the N_d factors in the product commute since defects never occur on neighboring triangles, and the variational parameter α determines the amount of next-nearest-neighbor singlets involved. For a single defect, the energy expectation of this new wave function turns out to be[9]

$$\Delta_\alpha = \frac{\frac{3}{4}+\frac{9}{4}\alpha+\frac{45}{16}\alpha^2}{1+\frac{3}{2}\alpha+\frac{9}{8}\alpha^2} \ . \tag{10}$$

The minimum, $\Delta_\alpha = \frac{1}{2}$, is achieved for $\alpha = -\frac{1}{3}$ and represents a significant improvement over the "bare" defect energy $\Delta_0 = \frac{3}{4}$.

The overlap and Hamiltonian matrix elements are now polynomials of α, but we can still use the small expansion parameter ϵ to specify the order of each matrix element. With the prescription given by Eq. (4) and Eq. (5), the computation of these matrix elements is straightforward, though tedious. Explicit formulas for both the overlap and energy matrix elements to the lowest nontrivial order $O(\epsilon)$ can be found in Ref. 9. In this section, we still study the effect of the lowest-order resonance as in the previous section by setting all matrix elements of order $O(\epsilon^2)$ and higher to zero. Effects due to higher-order resonances are investigated in Sec. VI. A numerical diagonalization is carried out for the same 36-spin cluster within the new basis. The ground state energy E_0 as a function of the variational parameter α is plotted in Fig. 6.

The optimal ground state energy $E_0 = -0.4380$ is obtained for $\alpha = -0.5$, which shows a remarkable improvement over -0.4089 found for the basis of dimerized states, and compares surprisingly well with the exact result -0.4383. Moreover, the significant shift in α, from -0.333 for a single defect, or a set of noninteracting defects, to the present -0.5, implies that a strong defect-defect interaction captured by this new variational wave function plays an important role in lowering the energy.

The energy spectrum of the first 100 lowest eigenstates and their corresponding average number of perfect hexagons for the basis with the optimal $\alpha = -0.5$ are plotted in Fig. 7 and Fig. 8, respectively. Compared with the basis of dimerized states ($\alpha = 0.0$) in Fig. 3, the magnitude of the gap has doubled, indicating an enchancement of the condensation described in the previous section. The defect-defect interaction appears to be attractive as in the previous section.

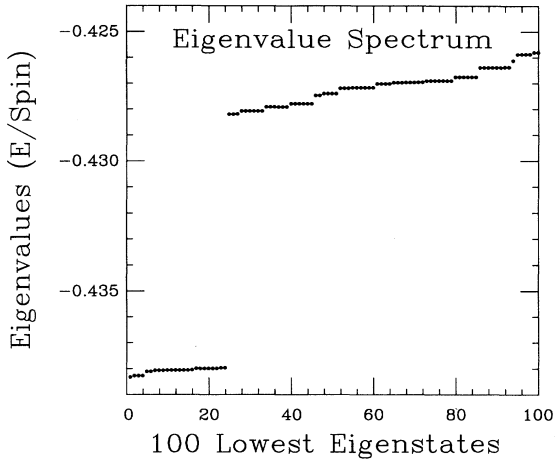

FIG. 7. The energy spectrum for the 100 lowest eigenstates for $\alpha = -0.5$. The energy has been converted to the conventional definition.

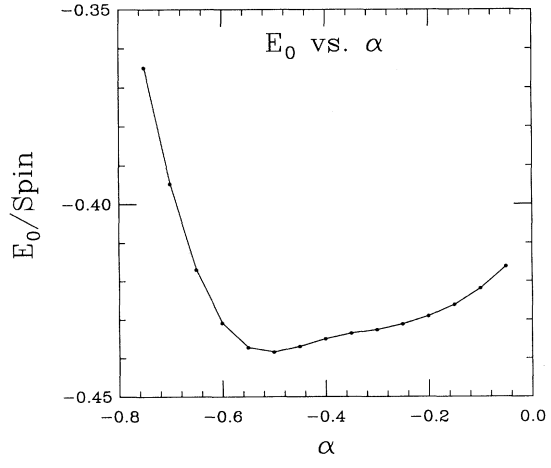

FIG. 6. The ground state energy E_0 per spin as a function of the variational parameter α. The energy has been converted to the conventional definition.

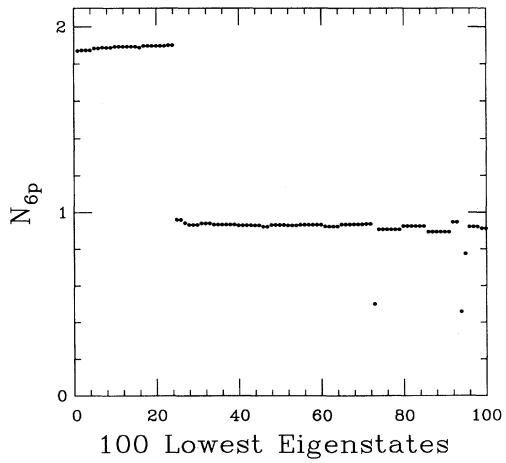

FIG. 8. The average number of perfect hexagons N_{6p} corresponding to the energy eigenstates of Fig. 7.

VI. HIGHER-ORDER RESONANCE

As discussed above in Sec. I, longer resonance loops induced by the nonorthogonality of the dimerized states are unavoidable. Therefore, the set of tunneling amplitudes $\{h_r\}$ in Eq. (7), associated with the lowest-order resonance loops, ought to be treated as phenomenological parameters at best—anticipating the renormalization from longer resonance loops. However, it is virtually impossible to explore such an eight-dimensional parameter space with all the competing energy scales. Instead, we take a more direct approach to numerically compute the overlap and Hamiltonian matrix elements to all orders of resonance for the 36-spin cluster.

All the translational and rotational symmetries of the 36-spin cluster have been used to make the numerical computation feasible. The reduced Hilbert space with dimension=2048 is further decomposed as

$$\begin{aligned}\Gamma(2048) = {} & 21\Gamma_1(1) \oplus 21\Gamma_2(1) \oplus 13\Gamma_3(1) \oplus 13\Gamma_4(1) \\ & \oplus 30\Gamma_5(2) \oplus 22\Gamma_6(2) \oplus 51\Gamma_7(3) \oplus 35\Gamma_8(3) \\ & \oplus 35\Gamma_9(3) \oplus 51\Gamma_{10}(3) \oplus 85\Gamma_{11}(6) \oplus 85\Gamma_{12}(6) \\ & \oplus 31\Gamma_{13}(2) \oplus 31\Gamma_{14}(2) \oplus 54\Gamma_{15}(4) \ , \end{aligned} \tag{11}$$

where the multiplicities and dimensions of the irreducible respesentions Γ_i $(i = 1, 2, \ldots, 15)$ are given with the dimensions indicated in parentheses.[11] This decomposition clearly shows that the dimension of the largest matrix encountered in diagonalization is 85.

For the basis of dimerized states $\{|D\rangle\}$ discussed in Sec. III, we study the effect of resonance order by order. For example, resonance to the nth order is taken into account by keeping all the matrix elements up to order $O(\epsilon^n)$ in both the overlap and Hamiltonian matrices and setting the rest to zero. For this sequence of truncations, we tabulate in Table I the corresponding ground state energy and the average number of perfect hexagons in the ground state. Clearly, the number of perfect hexagons drops from about 1.9 at the lowest order of resonance to a vanishingly small value when the fourth-order resonance loops and beyond are taken into account. The disappearance of the perfect hexagons in the ground state when higher-order resonance loops are included indicates that the nature of the defect-defect interaction has been *reversed* from being attractive (maximum numbers of perfect hexagons) to being repulsive (no perfect hexagons). Thus the condensed phase obtained at lowest-order calculation becomes unstable against higher-order resonance effects.

TABLE I. Ground state energy E_0 and average number of perfect hexagons in the ground state for each order of resonance for $\alpha = 0$.

Order	E_0/spin	$\langle N_{6p} \rangle$
0	-0.37500	0,1,2[a]
1	-0.39681	1.90013
2	-0.40258	1.67114
3	-0.40385	1.52118
4	-0.40530	0.06787
5	-0.40653	0.05712
6	-0.40713	0.05844

[a] Number of prefect hexagons allowed for a fully dimerized state of the 36-spin cluster in Fig. 1.

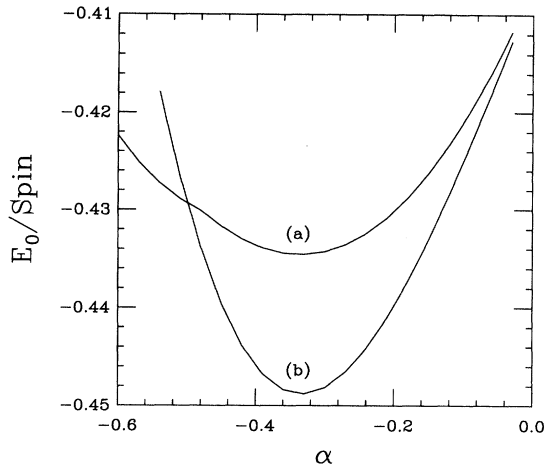

FIG. 9. (a) Ground state energy E_0 per spin as a function of α when all orders of resonance are included. The minimum is located at $\alpha = -0.329$. Curve (b) corresponds to the energy in Eq. (10) of noninteracting defects.

A similar calculation was performed for the basis $\{|D_\alpha\rangle\}$ introduced in Sec. IV. All the results reported hereafter are obtained by including all resonance loops. The ground state energy as a function of the variational parameter α is shown in Fig. 9 along with the energy in Eq. (10) for a set of noninteracting defects. The minimum energy, $E_0 = -0.4345$ per spin, is achieved for $\alpha = -0.329$ which is very close to the optimal value $\alpha = -\frac{1}{3}$ for a single defect, suggesting that the energy lowering comes from individual defects rather than defect clusters in contrast to the conclusion of the lowest-order calculations. This would be expected if defects are well

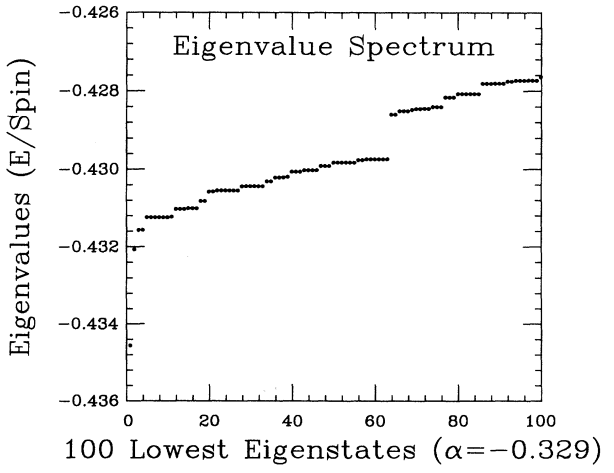

FIG. 10. The energy spectrum for the 100 lowest eigenstates for $\alpha = -0.329$ with all orders of resonance included.

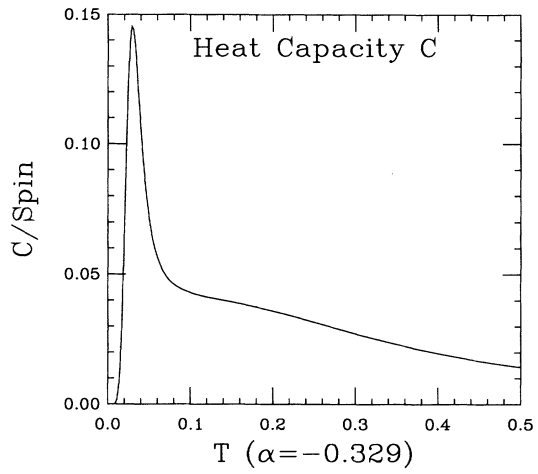

FIG. 11. Heat capacity per spin obtained for $\alpha = -0.329$ with all orders of resonance included.

separated from one another as a result of repulsive defect-defect interactions. Therefore, higher-order resonances appear to work against the formation of the hexagonal defect clusters. However, a crossover phenomenon occurs at about $\alpha = -0.5$, as clearly seen in Fig. 9, where the defects exhibit an attractive interaction when a larger amount of next-nearest-neighbor singlets are incorporated in the basis. This interesting finding is quite consistent with the results obtained by the low-order calculation where the energy minimum is achieved in the attractive defect-defect interaction regime.

The energy spectrum of the first 100 lowest eigenstates and its corresponding heat capacity are plotted in Fig. 10 and Fig. 11, respectively, for $\alpha = -0.329$. One interesting observation, besides the downward shift in temperature of the peak location to about $0.025J$, is the magnitude of the peak value which is almost double that of the $\alpha = 0$ case (see Fig. 5). This peak is well separated from the high temperature peak obtained by other means, for instance, the decoupled-cell Monte Carlo simulation[10] and the high-temperature expansion,[6] and thus strongly supports the double-peak feature in the heat capacity.

VII. CONCLUSION

Apart from the computational convenience inherent in discarding a large part of the Hilbert space, restriction to the short-ranged singlet pairs for the *kagomé* HAF is particularly well justified. A variational wave function, for example, composed of the nearest-neighbor singlet pairs and a relatively small amount of the next-nearest-neighbor singlet pairs has a rather favorable upper bound for the ground state energy, i.e., $E_0 = -0.4345$ per spin for the 36 spin cluster when all the resonances are included. This is only 1% higher than the exact energy $E_0 = -0.4383$.

The picture of the ground state at lowest order of resonance was considerably altered by the higher-order resonances. The appearance or disappearance of the perfect hexagons in the ground state, or equivalently the attractive or repulsive defect-defect interactions, for instance, appear to fall into two distinct regimes depending on the variational parameter α, i.e., the amount of next-nearest-neighbor singlets included. It is not clear at present whether these features are due to finite-size effects. In a small system, higher-resonance loops can easily take advantage of the periodic boundary conditions, giving unphysically large contributions to the overlap and Hamiltonian matrix elements.

Despite the uncertainty on the precise nature of the ground states when all orders of resonance are included, it is safe to say that the ground state will be a highly correlated spin liquid, if the translational symmetry is restored by the resonance. Moreover, the excitation energy scales in the singlet sector will be very small.

* Electonic address: chen@lanczos.ma.umist.ac.uk

[1] D. Rokhsar and S. Kivelson, Phys. Rev. Lett. **61**, 2376 (1988).
[2] P.W. Leung and V. Elser, Phys. Rev. B **47**, 5459 (1993).
[3] R.R.P. Singh and D. Huse, Phys. Rev. Lett. **68**, 1766 (1992).
[4] B. Bernu, P. Lecheminant, C. Lhuillier, and L. Pierre, Phys. Scr. T **49**, 192 (1993).
[5] V. Elser, Phys. Rev. Lett. **62**, 2405 (1989).
[6] N. Elstner and A.P. Young, Phys. Rev. B **50**, 6871 (1994).
[7] D. Rokhsar, Phys. Rev. B. **42**, 2526 (1990).
[8] J.B. Marston and C. Zeng, J. Appl. Phys. **69**, 5962 (1991).
[9] V. Elser and C. Zeng, Phys. Rev. B **48**, 13647 (1993).
[10] C. Zeng and V. Elser, Phys. Rev. B **42**, 8436 (1990).
[11] J.F. Cornwell, *Group Theory in Physics* (Academic Press, New York, 1984), Vol. 1, Chap. 9.